Dynamic optimization of two methods of the long jump

by

Stacy Mo

Submitted to the Department of Mechanical Engineering
in partial fulfillment of the requirements for the degree of

Bachelor of Science in Mechanical Engineering

at the

MASSACHUSETTS INSTITUTE OF TECHNOLOGY

June 2017

Signature redacted

Author .....
Department of Mechanical Engineering
May 12, 2017

Signature redacted

Certified by .....
Sangbae Kim
Associate Professor
Thesis Supervisor

Signature redacted

Accepted by .....
Rohit Karnik
Associate Professor of Mechanical Engineering
Undergraduate Officer

Dynamic optimization of two methods of the long jump

by

Stacy Mo

Submitted to the Department of Mechanical Engineering
on May 12, 2017, in partial fulfillment of the
requirements for the degree of
Bachelor of Science in Mechanical Engineering

Abstract

In this thesis, I analyzed, modelled, and optimized two different techniques of the long jump: the hitchkick and hang. Using video data, I made a dynamic model of both techniques, then created a cost function that took torques and angles into consideration to simulate physical limitations. Using a function minimizing optimizer, trajectories were simulated over a range of torque limits and angle penalties. Over the course of 292 simulations, we found that the hitchkick technique improved jump distances more than the hang technique, improving by up to 34.65% with an average of 7.7% while the hang technique increased jump distance by a maximum of 30.21%, with an average of -15.89%.

Thesis Supervisor: Sangbae Kim
Title: Associate Professor

Acknowledgments

I would like to thank Albert Wang, for his guidance, patience, and mentoring during this project and beyond. I would also like to thank Professor Sangbae Kim, for his advice and support during the past year working in his lab.

Special thanks to my family- Mom, Dad, Swansea, and Adrian- for the love and support during my time at MIT.

Additional thanks to Cyndia Cao and David Doan for all the love, food, and support given during the process of creating this thesis. And finally, I would like to thank Michelle Chen for always being there with coffee or company, even regardless of how late into the night I am working.

Contents

1 Introduction **13**

2 Background **15**

2.1 Long Jump 15

2.2 Biomimetics and Human Motion 16

3 Experimental Design **19**

3.1 Model of the Body 19

3.2 Mathematical Model 20

3.3 Video Analyis 21

3.4 Computer Model 22

3.5 Optimization 24

3.5.1 Optimization Parameters 27

4 Results **33**

5 Conclusions and Future Work **37**

A Anthropomorphic Data for the Human Body **39**

B Dynamics of a four-link unconstrained uystem **41**

List of Figures

2-1 Schematic of the long jump phases. 17

3-1 Body modeled after four links 20
3-2 Tracker interface and data collection 22
3-3 Data-fitted trajectory vs. torque-derived trajectory. 23
3-4 Flow chart of simulation process. 25
3-5 Optimization of torque functions compared to that of torque tapes. . 28
3-6 Spread of hitchkick optimization parameters and resulting distances. . 29
3-7 Spread of hang optimization parameters and resulting distances. . . . 30
3-8 Hitchkick optimization results from angle penalties of a 1E-5 multiplier 32

4-1 Physically feasible result of an optimized hitchkick jump. 34
4-2 Hitchkick optimization compared to hang optimization 35
4-3 Histogram of hitchkick and hang results. 36

List of Tables

3.1 Physical properties of links 21

3.2 Angle function fits and R-squared values for the hitchkick and hang technique. 23

A.1 Anthropomorphic Data. 39

Chapter 1

Introduction

Studying biomechanics of humans and other organisms has been of interest especially for dynamic models and robots. Understanding the dynamics of everyday motion has helped inform models and more accurately establish control systems for robots. The development of legged robots in the past decades have dramatically increased research in this area.

Current quadruped and bipedal robots are limited to basic locomotion: walking and running. However, humans and quadrupeds are capable of much more, such as jumping, and these motions generally follow a pattern. In the case of human jumping for distance, the technique to maximize distance travelled has been well practiced and perfected by athletes. As one of the original Olympic events, the long jump event has been a competition for centuries. However, there are several techniques jumpers use in the air to extend their jump, of which two are consistently used by elite jumpers.

In this thesis, we investigate the dynamics of two different long jump techniques and compare their effectiveness and ability to improve. The hitchkick technique features the athlete running through the air, while the hang technique has minimal leg movement. The two techniques are completely opposite in what the athletes do, but neither has been proven to have an advantage over the other.

Chapter 2

Background

2.1 Long Jump

As with most track and field events, the long jump is straightforward in its goal to jump the farthest. However, there are many techniques and nuances that go into the multiple phases, with several different methods for each. The long jump can be split up into four phases: run up, takeoff, flight, and landing. Each presents different motions, and dynamically, different conditions for the optimal jump.

The approach focuses on increasing momentum and maximizing height, which is relatively straightforward. There are three main objectives: a large horizontal velocity, a large decrease in center of gravity near the end of the approach, and accuracy in the length of the run-up. There is a linear relationship between horizontal velocity and distance of the jump, because in flight, momentum defines how quickly through the air the athlete travels. Since running speed and lowering the center of gravity (done in the penultimate step) are relatively easy to master, most jumpers actually spend time on being consistent with their approach length [4].

Take-off, on the other hand, presents many complications along the entire body; anything from the placement of the arms to the ground reaction forces can make a significant difference in the jump. Being in contact with the ground presents the challenge of external forces, as athletes try to push off the ground as forcefully as possible to increase vertical velocity. Different models, such as a 17-link model including the

main muscles have been used to simulate the internal torques and motion of the body at take-off [3]. Other studies have focused more specifically on the ground reaction forces related to takeoff. Reaction forces rapidly change over the course of the plant, where jumpers step forcefully on the jump board. Overall, the greater the force, the farther the jump [11].

In flight, the center of mass of the jumper flies like a mass in projectile motion. However, jumpers still have angular momentum about the center of mass. To increase jump distance, athletes contort themselves such that their legs are as far out and horizontal as possible to prepare for landing. To do so, jumpers either eliminate this rotation outright, and hang (appropriately called the hang technique) or run in the air, called a hitchkick [4]. There has been little proof on a definitive best technique, but there is one conventional landing position that has been proven to increase jump distances. This landing position has the torso leaned forward reaching for their toes, as horizontal as possible. Momentum of the body slides the rest of the body to the point where the feet made contact with the ground, so even though most of the body is behind the point of ground contact initially, distance is still maximized as the body reaches zero velocity [5].

2.2 Biomimetics and Human Motion

Studying locomotion of legged organisms has been of interest to scientists in understanding the dynamics. This has been helpful in computer modelling and simulation, and in a physical application mimicking the movement of organisms helps dictate the movement of mechanisms. Legged robots also have an advantage over wheeled vehicles on uneven terrain, including stairs [10]. Quadrupeds have been the most developed of legged robots, given their higher stability by quantity of limbs and thus decreased need for high-speed feedback. The study of quadruped locomotion dates back to 1878, when Eadweard Muybridge first took a succession of a galloping horse. Since then, successful quadruped robots include Boston Dynamics Big Dog and the MIT Biomimetics Labs Cheetah.

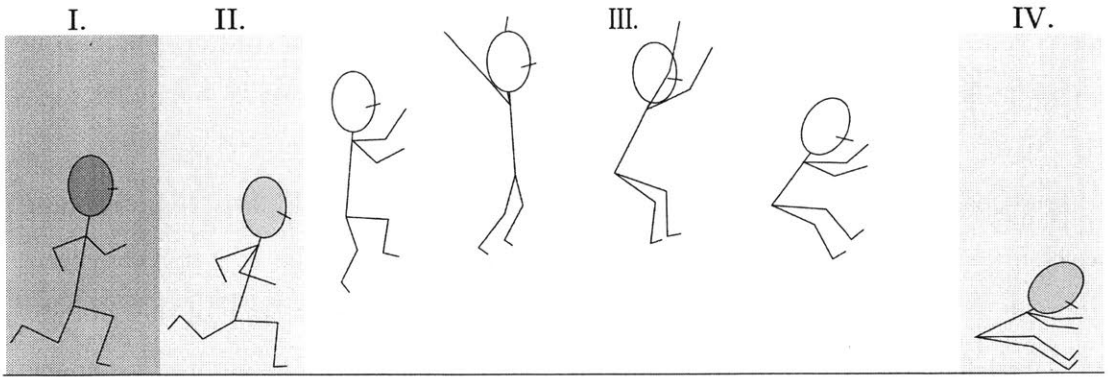

Figure 2-1: **Schematic of the long jump phases.** Phase I represents the approach, where the jumper runs down the runway to gain momentum. The step before hitting the board is dedicated to lowering the center of gravity to increase the impact of the next step. Phase II is the takeoff phase; jumpers stomp the ground as hard as possible to increase impact an upward velocity. Phase III is the flight phase, where the jumper sails through the air and contorts themselves to prepare for landing. Finally, Phase IV is the landing phase, where jumpers try to maximize their distance by stretching their legs out.

Human motion has also been extensively studied. However, bipedal motion presents a more difficult challenge: there are higher degrees of freedom, and especially in the case of contact with the ground, more nonlinear dynamics are present. Bipedal motion has been mainly centered around walking, but given the multiple phases of walking, quantifying the gait is complicated. In walking, there is a step off (one-legged), impact (heel strike) and double support (both legs). Each case presents different conditions based on reaction force and center of gravity, which in turn effects the stability of the system [10].

Models have been developed for cases where there is no ground contact. In these cases, the center of mass will follow a parabolic curve (with gravity), and angular momentum is conserved [1]. In zero gravity cases, external limbs are used by astronauts to help reposition the body as needed. By producing pitch and yaw, the body can self-rotate. This is also easily applied to non-living bodies, such as satellites, where repositioning is crucial to functionality [9].

With gravity, there exist models for somersaults and backflips, both of which are limited to short time frames before the person reaches the ground again. However,

this is more applicable especially when building a robot modelled after a human in the sagittal plane, and has successfully been modelled and created on a smaller scale [7].

Free space dynamics have also been of interest in cats with their re-positioning method, which always results in landing feet-first regardless of the direction they were dropped in. By simplifying the cat into a two-linked mass, the motion of the cats was quantified dynamically after they were dropped upside-down [8]. Similarly, models of humans have been done on three and four-linked models, decomposing the human body into sections of legs, torso, and arms. This serves as a sufficient simplification of human complexity for dynamic modelling, especially in free space, where there is no contact with the environment [6].

Chapter 3

Experimental Design

3.1 Model of the Body

Several studies on human motion have simplified the complexity of the human body to linked masses. For a planar body in the sagittal plane, this usually combines the torso with the head, the upper arms and the forearms, and the foot with the leg. These, combined with the thigh, create a four-linked system that can be used to model dynamics. Some models consider the arms as negligible, consolidating the arms to the torso and using to a three-link model. In the case of long jump, the arms play a significant role, increasing jumps by an average of 21.2% in a standing long jump [2]. Thus, a four-link model was used for this model.

Links 1, 2, 3, and 4 correspond to the leg, thigh, torso, and arms, respectively. The general coordinates for the system are for the center of mass (x_g, y_g), ankle position (x_0, y_0), and angles at the ankle, knee, hip, and shoulder $(\theta_1, \theta_2, \theta_3, \theta_4$, respectively). θ_1 corresponded to the ankle angle with respect to the environment, whereas θ_2, θ_3, and θ_4 are in the body frame (in relation to the surrounding links to the joint). It is assumed that the torques act at these joints, which are τ_1, τ_2, τ_3, and τ_4, respectively. In flight, we assume τ_1 to be zero since the body is not in contact with the environment. Derivations of values for mass fractions, center of mass location per link, and moment of inertia from Table 3.1 are calculated using anthropomorphic data and explained in detail in Appendix A.

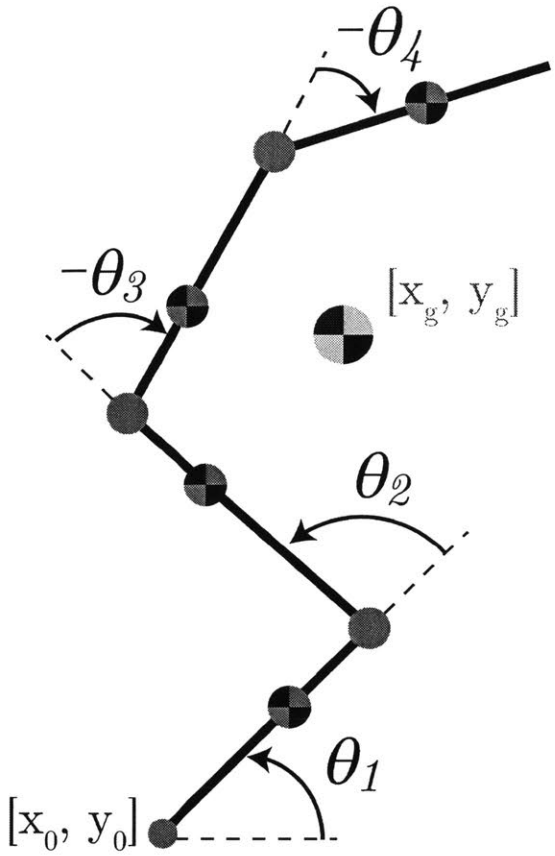

Figure 3-1: **Body modeled after four links.** Each link represents the leg, thigh, torso, and arm. The point $[x_0, y_0]$ corresponds to the ankle location, and (x_g, y_g) represents the location of the overall center of mass.

3.2 Mathematical Model

Using Lagrange equations of motion, the generalized coordinates used are $q_g = [x_g, y_g, \theta]^T$, with $\theta = [\theta_1, \theta_2, \theta_3, \theta_4]^T$. Given the lack of contact with external forces such as the ground in the flight phase, the dynamics for the body at this point is simply

$$J_g(q_g)\ddot{q}_g + H_g(q_g, \dot{q}_g) + G_g(q_g) = u \tag{3.1}$$

where u represents the force vector corresponding to the torques on the joints.

$$u = [F_x, F_y, \tau_1, \tau_2, \tau_3, \tau_4] \tag{3.2}$$

Table 3.1: **Physical properties of links.** Mass, length, center of mass (proximal) and moment of inertia used for data modelled after Tianna Bartolletta, female long jump gold medalist in the 2016 Olympics. Derivations for each part are in Appendix A.

Link	Mass (kg), m	Length (m), l	Distance to COM (m), l_c	Moment of Inertial (kg/m^2), I
Link 1 (Leg)	7.4707	0.4132	0.1628	0.4187
Link 2 (Thigh)	12.2470	0.3892	0.2206	0.1935
Link 3 (Torso)	35.3938	0.7778	0.2644	7.8925
Link 4 (Shoulder)	6.1235	0.6878	0.3645	1.2060

The matrices for Jg, the inertial matrix, Hg, the non-linear term, and Gg, the gravitational matrix, are detailed in Appendix B [7].

3.3 Video Analyis

Videos of Olympic jumpers from Rio 2016 were analyzed with Tracker, an open source video analysis tool. Locations of the ankle, knee, hip, shoulder, head, elbow, and hand were taken over the course of the flight phase and set to an origin point that was present in the entirety of the analyzed phase as the origin. For these particular videos, the four-meter mark was set as the origin and then compensated for later during the data analysis in MATLAB. Points were chosen by inspection or found using a pattern-matching search in Tracker, which took color patterns and matched them to the next frame to find where the object moved. Because of the limited size of the frame, data analysis usually started a couple frames after the athlete had taken off and went until contact with the ground was made. From there, the data points were exported to MATLAB for further analysis.

Given the angle the cameras used for the videos were at, scales from the environment were taken in the horizontal direction. Any vertical landmarks on the ground would have been highly skewed, but assuming the cameras were very far away from the jump pit, it can be estimated that horizontal landmarks are unskewed and can be treated as such. However, the slight skew in camera angle actually changed the

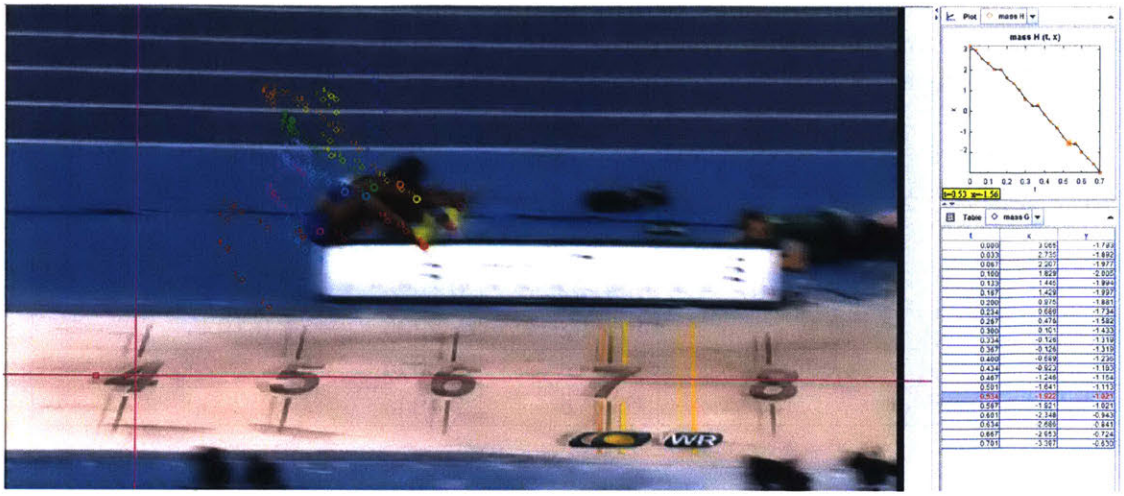

Figure 3-2: **Tracker interface and data collection.** Origin was placed at the 4m mark and skewed as necessary.

dynamics because of the scaled vertical image. Because the vertical scale was slightly smaller than that of the horizontal, this resulted in an unknown upward force after calculating torques from the data. This was resolved by multiplying the vertical coordinate by the tangent of the angle of the camera to unskew the vertical compression.

3.4 Computer Model

In the model, we are looking for the greatest distance travelled by the jumper. To replicate the dynamics of the jumper, location data from Tracker was taken into MATLAB then normalized to compensate for the origin offset. These were then converted to the generalized coordinates q_g and solved for torques. For each jumper, there were 3-4 different jumps from which data was extracted from to compare to. From these sets of data, functions were fitted to the θs over time using MATLAB fit function. The angle data fit 3^{rd} to 7^{th} order polynomials as described in Table 3.2. The τ vectors were obtained by using the θ fit, q_g, and solving the dynamics equations described above. This output τ was used as the seed value in the optimization, a baseline for the general torques experienced in our model derived from data.

The model was able to reasonably replicate the trajectory of the jumper after deriving torques and using them to re-calculate the trajectory. There were some

	Angle	Polynomial Fit	R-squared
Hitchkick	θ_1	5^{th} degree	0.9279
	θ_2	5^{th} degree	0.6093
	θ_3	3^{rd} degree	0.9207
	θ_4	3^{rd} degree	0.6098
Hang	θ_1	4^{th} degree	0.9314
	θ_2	7^{th} degree	0.8340
	θ_3	5^{th} degree	0.9526
	θ_4	4^{th} degree	0.9517

Table 3.2: **Angle function fits and R-squared values for the hitchkick and hang technique.** Hitchkick technique data was taken from Tianna Bartoletta, and hang technique data from Brittney Reese.

discrepancies, however, as seen in Figure 3-3. This may be due to the fact that not every jump by that particular athlete is identical, so in averaging the general trajectory and motion of the athlete, some detail may have been lost. And although there are many studies on the biomechanics of the human body in the area of centers of mass and mass, different people have different distributions of weight throughout the body, which may also contribute to inaccuracies in the model.

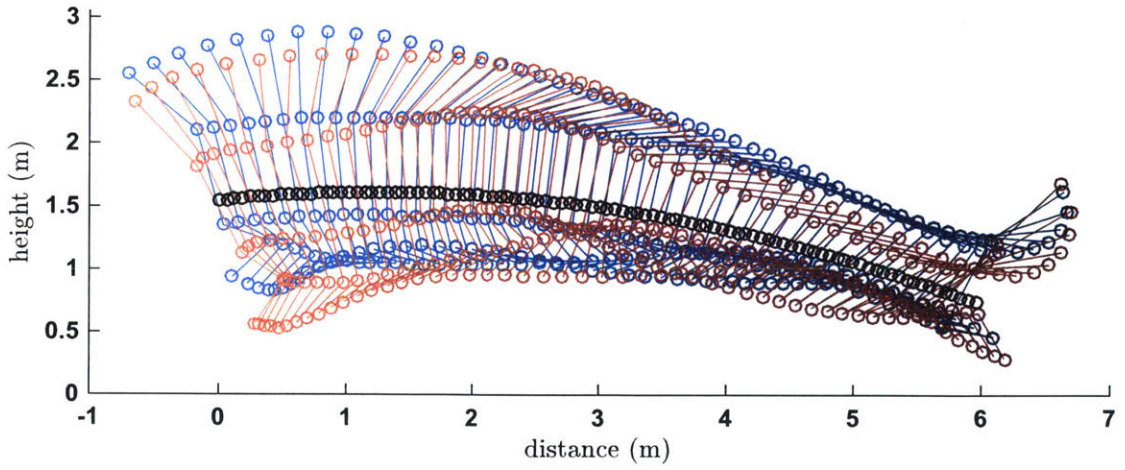

Figure 3-3: **Data-fitted trajectory vs. torque-derived trajectory.** The red represents the data fit, and the blue represents the torque-derived trajectory. As seen here, there is some discrepancy between the data and derived trajectory. The derived trajectory was created by fitting the angles from the data, calculating torques, then inverse-calculating the angles back again.

In the interest of also comparing different jumping techniques, this analysis of angles and torques was done on two different jumpers with different techniques. Two different jumpers, Tianna Bartoletta and Brittney Reese, were analyzed from 2016 Olympic footage. Both received a gold and silver medal in the long jump that year, and Bartoletta utilized the hitchkick technique while Reese uses the hang method. Thus, both styles were modeled then run through the optimizer and compared.

3.5 Optimization

Optimization was done with MATLAB function *fmincon*. This function works by taking the minimum of a defined cost function, f_c:

$$min f_c(\vec{\tau}, \vec{q_{g0}}) \tag{3.3}$$

$$s.t. \vec{\tau} = [\tau_{ankle,1}, \tau_{ankle,1}, \tau_{knee,1}, \tau_{hip,1}, \tau_{shoulder,1}, \tau_{ankle,2}, \cdots \tau_{shoulder,end}] \tag{3.4}$$

$$\tau_{min,ankle} \leq \tau_{ankle,i} \leq \tau_{max,ankle} \tag{3.5}$$

$$\tau_{min,knee} \leq \tau_{knee,i} \leq \tau_{max,knee} \tag{3.6}$$

$$\tau_{min,hip} \leq \tau_{hip,i} \leq \tau_{max,hip} \tag{3.7}$$

$$\tau_{min,shoulder} \leq \tau_{shoulder,i} \leq \tau_{max,shoulder} \tag{3.8}$$

where τ are the input torques and q_{g0} is the initial q-vector which contains the coordinates of the center of mass and angles of links at a given time. The cost function also takes angles and torques into account. If an angle on a specific link cannot exist on a human body, the optimizer penalizes unfavorable results so they are less likely to occur. Torques were either penalized in the same way as unfavorable angles or set as hard limits.

The cost function was given torques in two different ways. The first method involved fitting the seed torque data in polynomial fits and optimizing the coefficients of the variables of those functions. Optimizing the coefficients of the torque functions proved to limit improvements, since it constrained the torque functions to a specific

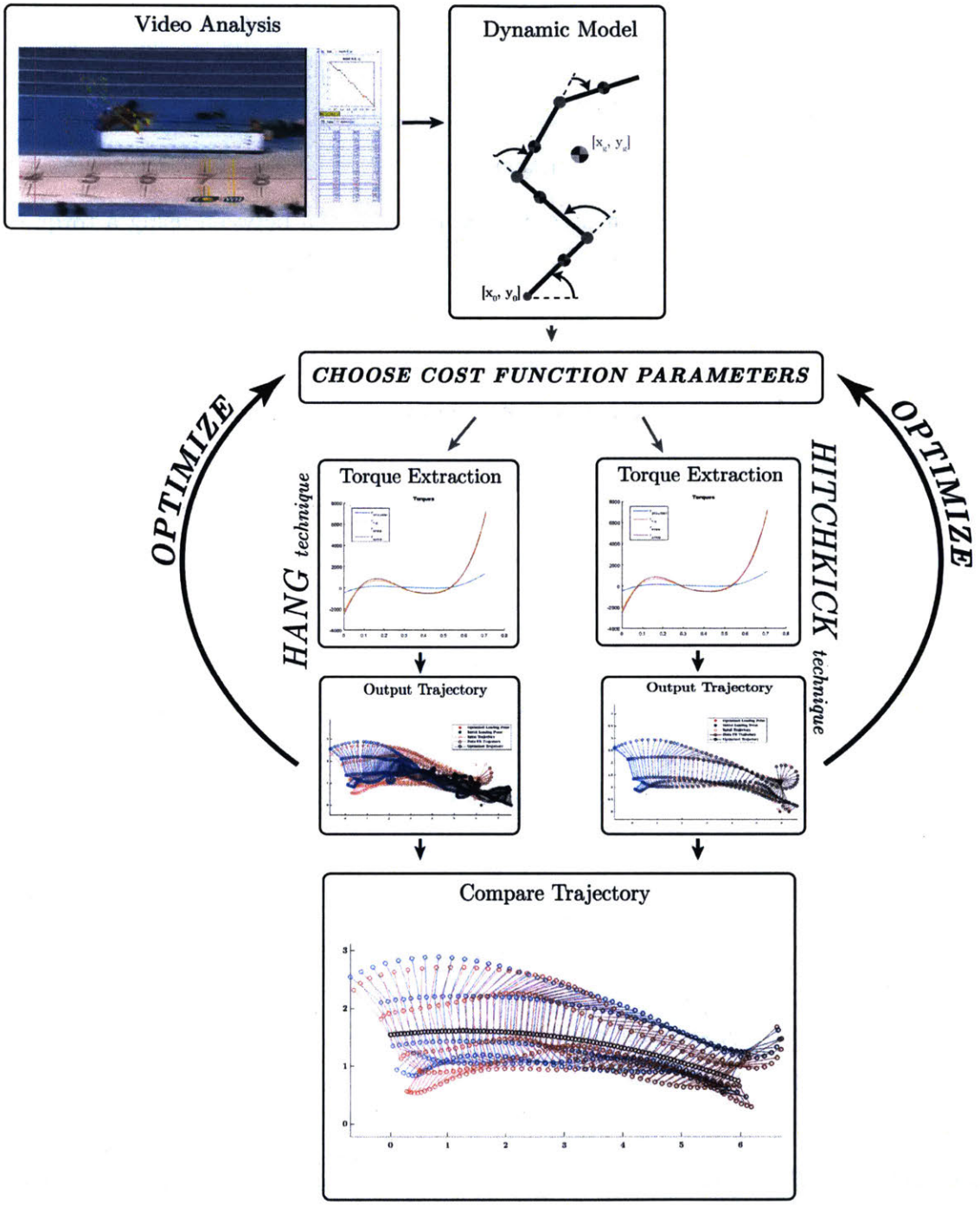

Figure 3-4: **Flow chart of simulation process.** A dynamic model was built, then data from video were used to give sample torques in the case of long jump flight. Trajectories were then calculated from these torques, and using a cost function minimizer the trajectory was optimized. The optimization step itself took fine-tuning to ensure a feasible and ideal solution. Results for the same limit and penalties were also the same.

shape which may not have necessarily been the most effective trajectory. Thus, a torque tape was used. Torque tapes are a "tape" of the torque function over a relevant amount of time. This increases flexibility by enabling the shape of the torque outputs to not be constrained to a specific function type.

Different penalties resulted in different results, and even between using a torque tape versus a torque function there was variation in the distance jumped. Limits were placed on a range of torques, and penalties on angles of certain limbs. θ_1 and θ_4, corresponding to the ankle and the shoulder, did not have limits set because the ankle angle (θ_1) is in reference to the environment (body can freely spin if necessary) and the arm (θ_4) can swing around fully because of the ball-joint nature of the shoulder. On the other hand, θ_2 and θ_3, corresponding to the knee and hip, respectively, were constrained. The ability to bend in the wrong direction is a strong indication that a limb is going through the torso or the leg is broken.

Penalties acted in the form of multipliers in the cost function or set as hard limits. The difference of the angle limit and the actual angle was taken, squared, then added over the course of the entire simulation to calculate the base of the angle penalty. This was then multiplied by the angle penalty multiplier (p_a), then added to the cost function output in an attempt to minimize the function:

$$cost = -distance + p_a \sum_{i=1}^{t} (\theta_0 - \theta(i))^2 \tag{3.9}$$

Given that the original model after being fit to the data still gave some impossible angles and incredibly high torques, the cost ranged from heavy penalties to seemingly trivial ones. When optimizing torques as coefficients of a function, the trajectories came out relatively stable and feasible. However, using a torque tape resulted in some very unstable trajectories; the body would flip around, and when angle penalties were added the jumps were shorter by almost a meter.

Additionally, different techniques resulted in different optimization issues and results. The hang technique was simpler to model, since the limbs of the athlete were relatively motionless, but the optimizer still had lots of issues preventing the body

from twisting wildly. On the other hand, the hitchkick is very active in nature as the jumper runs in the air. This method was more difficult to model, but the simulation was easier to control.

3.5.1 Optimization Parameters

The torque-tape model, given greater flexibility and speed, was ultimately chosen to optimize the jump. Adding torque penalties made the simulation in the coefficient model stall as the function minimizer struggled to find smaller values given the non-linear nature of the dynamics. Additionally, changes in the coefficients were still constrained to that particular torque function shape. However, in using the torque-tape, the minimizer had to be contained such that overly large torques and angles would not occur.

The simulation was run over a range of torques limits and angle penalties in an attempt to identify a trend for an optimal and feasible range to optimize around. Torques were limited from $\pm$2000Nm down to just $\pm$5Nm and angles were penalized with a multiplier of 1E-6 all the way up to 1E8. Between the hitchkick and hang technique, the simulation and optimizer was run a total of 292 times.

An analysis of 181 hitchkick simulations showed the greatest distances were generally towards the smaller torque limits, but not always. The higher torque ranges resulted in either very large distances or ones smaller than initial condition due to the size of the torque limits. Because of this wild variation, torques within [-500, 500] consistently improved the jump as opposed to making it worse. This also coincides with humanly-possible torques of around 200Nm [12].

Plotting the penalties and limits over the distance jumped resulted in many straight lines, as seen in Figures 3-6 and 3-7. This is due to the fact that after a certain point, increasing penalties to discourage certain behavior eventually overshadows the distance metric, and the optimizer would create very similar trajectories with similar distances. Thus, the best place to take optimization parameters is at the peak right before the plateau.

Limiting the torques also prevented the model from erratic behavior, resulting in

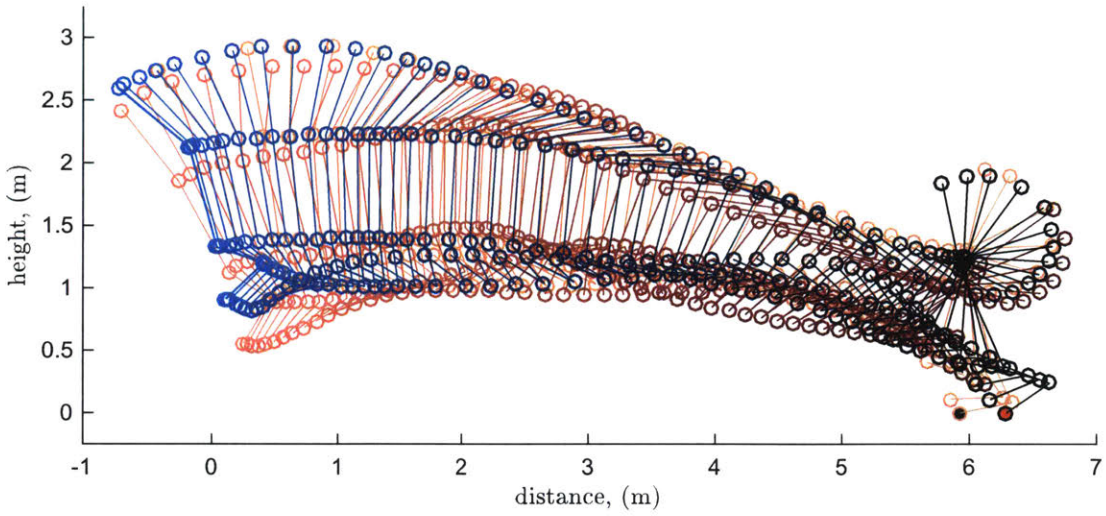

(a) Torque-function Method.

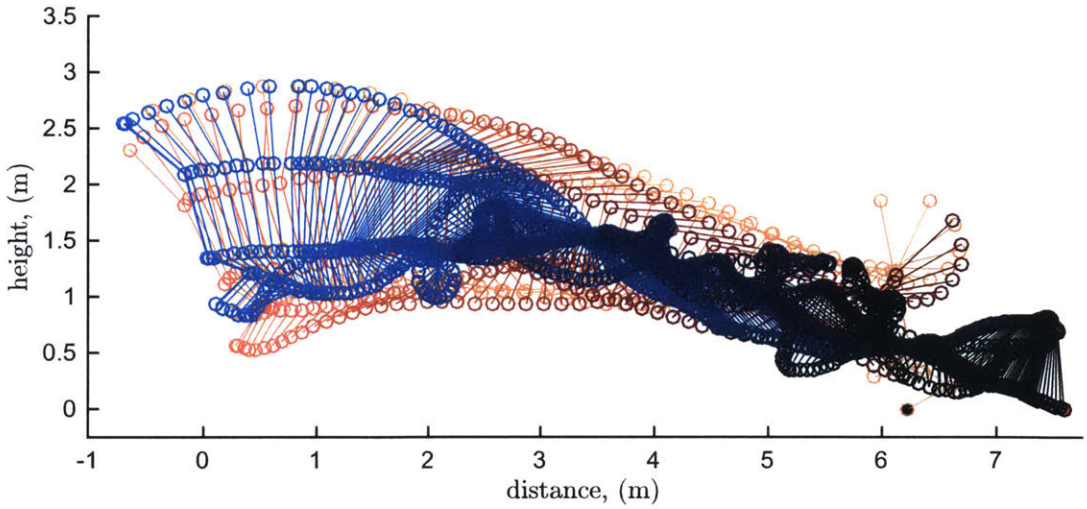

(b) Torque-tape method.

Figure 3-5: **Optimization of torque functions compared to that of torque tapes.** These simulations were done with no torque limits or penalties and an angle penalty of 1E-3. Clearly, torque tapes give more freedom to the model, and generally travel greater distances. Red represents the initial trajectory, orange the data-fit with functions, and blue the optimized trajectory. (a) Torque-function optimization method, with a final distance of 6.2908m. (b) Torque-tape optimization, with a final distance of 7.5881m.

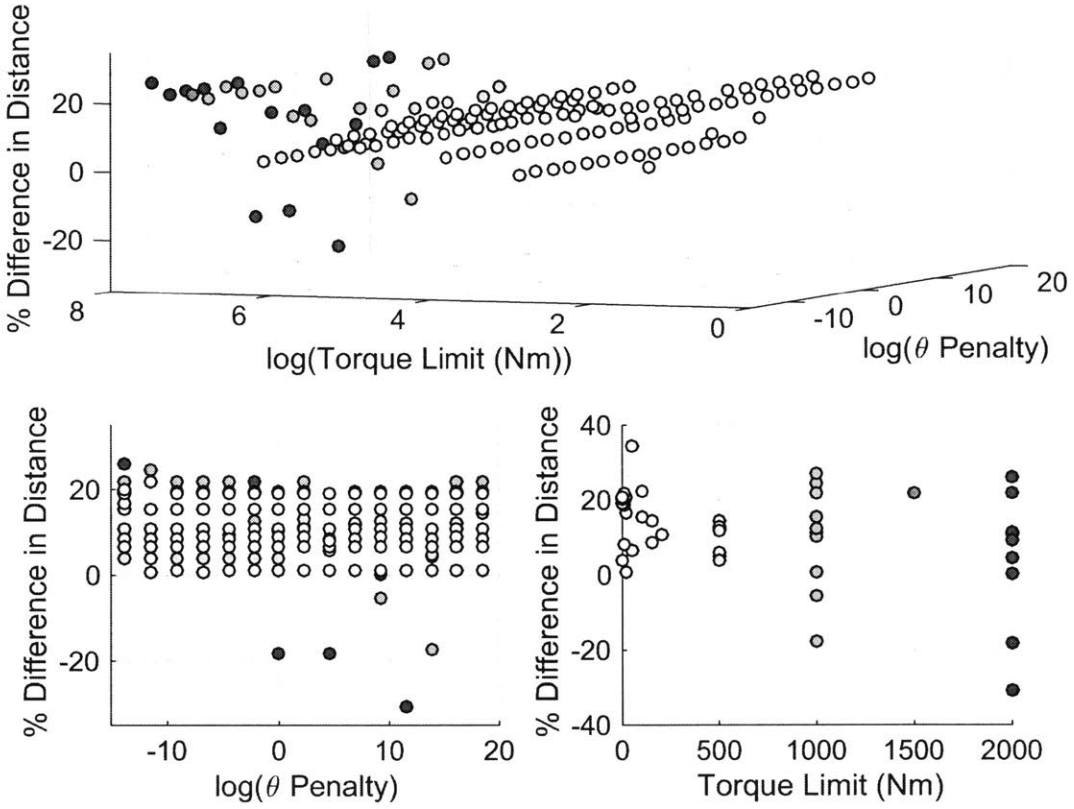

Figure 3-6: **Spread of hitchkick optimization parameters and resulting distances.** *Top:* 3D plot of the log of the angle penalty, log of torque limits, and percent difference of distance. The smaller the torque limit, the more consistent the results are, and given a lower torque limit the penalty does little to effect the distance jumped. *Bottom left:* log spread of the angle penalty compared to the percent difference in distance. *Bottom right:* Spread of torque limit over percent difference in distance jumped.

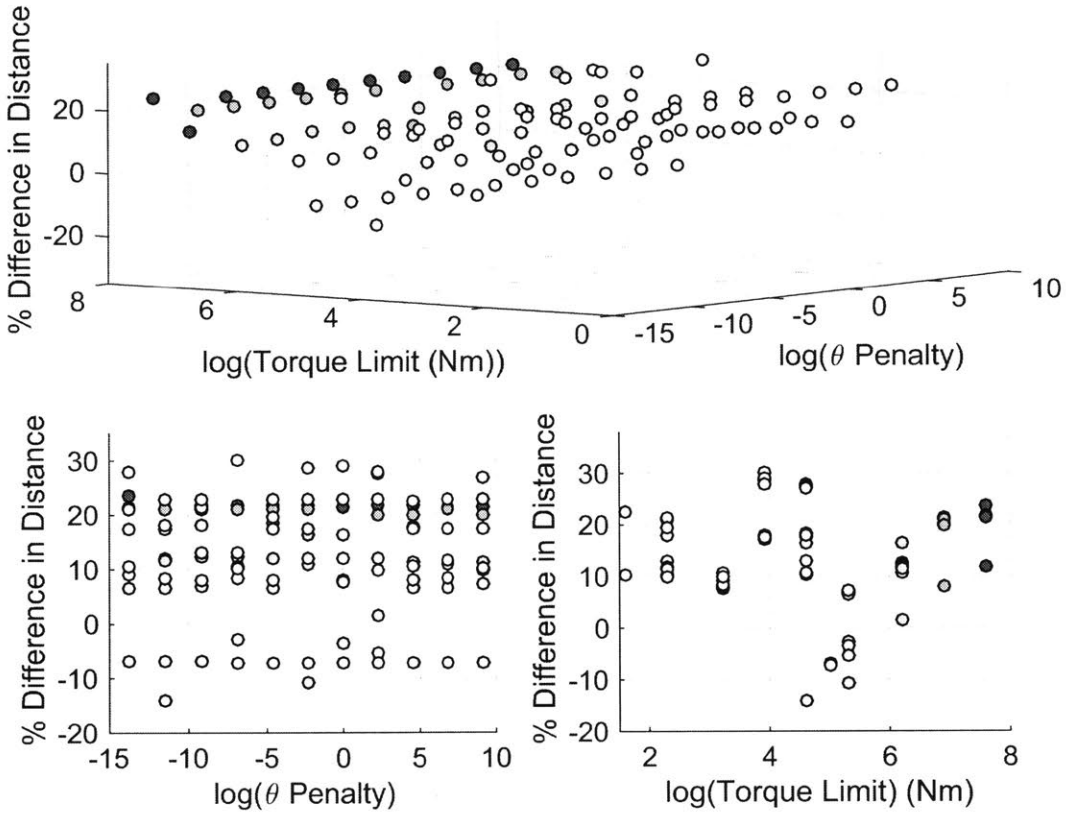

Figure 3-7: **Spread of hang optimization parameters and resulting distances.** *Top:* 3D plot of the log of the angle penalty, log of torque limits, and percent difference of distance. There is more variation in and less straight lines in these plot compared to the hang results, and it is clear that the same optimization parameters used for the hitchkick technique could no be used for the hang. *Bottom left:* log spread of the angle penalty compared to the percent difference in distance. *Bottom right:* Spread of torque limit over percent difference in distance jumped.

a smoother trajectory because the bodies were limited in speed given low torques. Additionally, the smoother trajectory looked more similar to what is already done in long jump because of the prevention of full body flips and segment spinning.

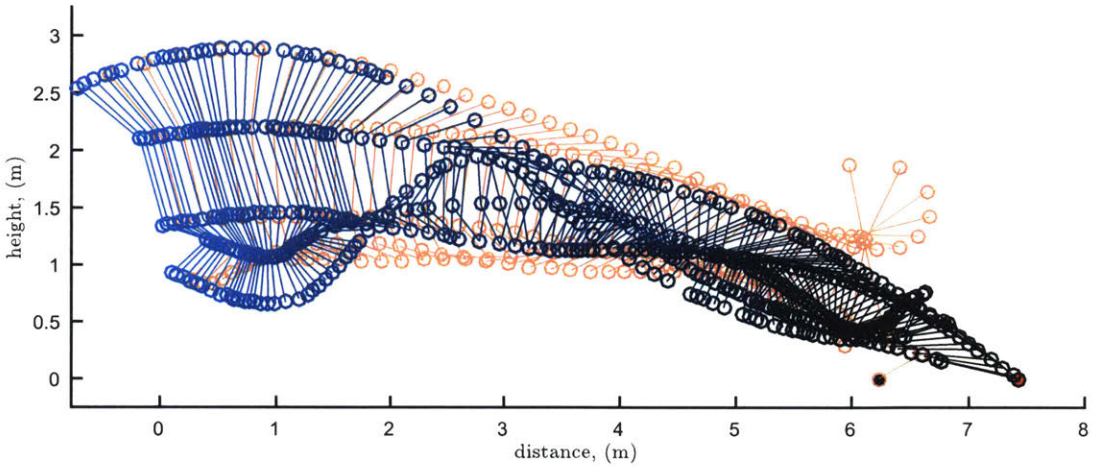

(a) Torque limit of [-10, 10] Nm, 7.4256m long.

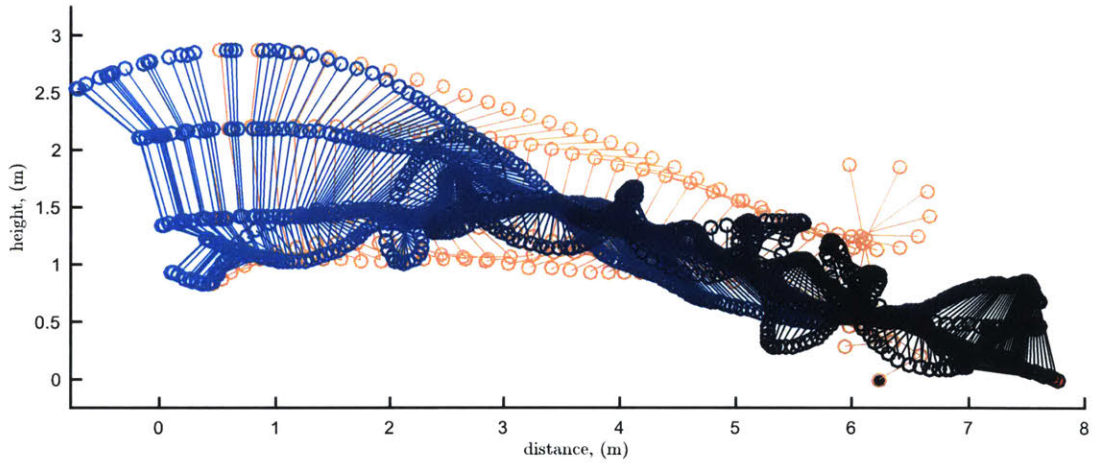

(b) Torque limit of [-1000, 1000] Nm, 7.7576m long.

Figure 3-8: **Hitchkick optimization results from angle penalties of a 1E-5 multiplier.** Orange timelapse represents the inital seed trajectory, blue represents the optimized timelapse; the black dot is the initial landing point, and the red dot is the optimizaed one. (a) Trajectory of a torque limit of [-10, 10] Nm. (b) Trajectory of a torque limit of [-1000, 1000]. These parameters resulted in the largest increase of distance given non-zero limits and penalties, with a 21.71% increase for 10Nm limit and 24.51% increase for the 1000Nm torque limit. However, it is clear that the smaller torque range is more feasible because of the slower motion: jumpers are in the air for less than a second, so wild spins would not be humanly possible.

Chapter 4

Results

Comparing the two types of jumps, the hitchkick technique resulted in higher distances. Although initial modelling of the hang technique appeared to be simpler, the hang technique became more warped than the hitchkick technique in simulations. Optimization parameters resulted in different outcomes depending on the technique, so the best hitchkick parameters were not the highest performing ones for the hang technique.

The hang technique averaged lower distance increases of -15.86% but still consistently increased distances by over 10% otherwise and is capable of increasing up to 20% with limits and penalties. Trajectories coming from the hang technique were incredibly warped and impossible for a human to perform them as seen in Figure 4-2. This may be due to the stationary nature of the technique, causing the ability for flexibility in torque tapes to twist the bodies.

In the hitchkick technique, however, distances were able to increase by over 30% given unbounded limits (no torque limits nor angle penalties) and otherwise consistently over 15% improvement. It also averaged an increase of 7.7%. The smoother, more reasonable trajectories, such as the one seen in Figure 4-1, normally did not go as far as more physically impossible simulations, but seem feasible while still being an improvement in distance.

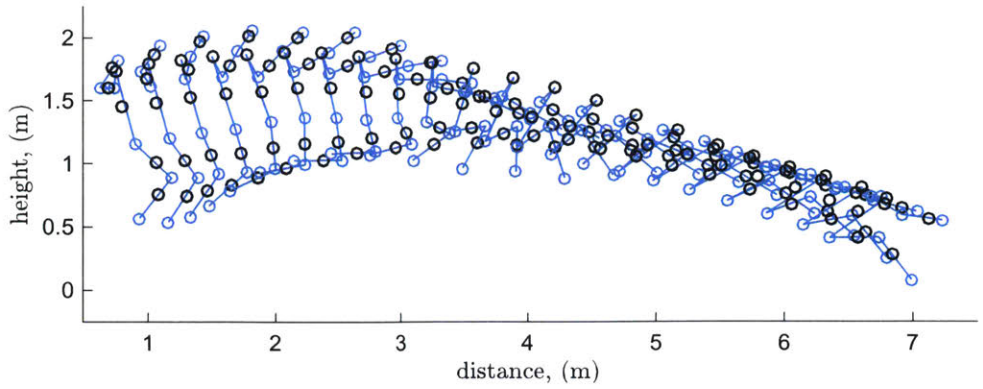

(a) Torque limit of [-10, 10] Nm, 7.4256m long.

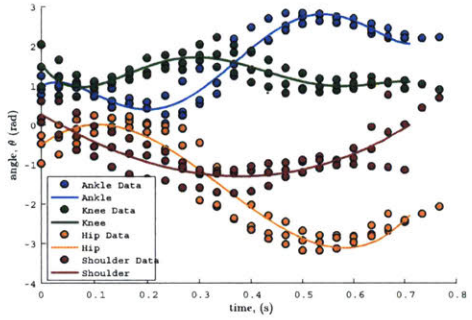

(b) Angle data and angle fits.

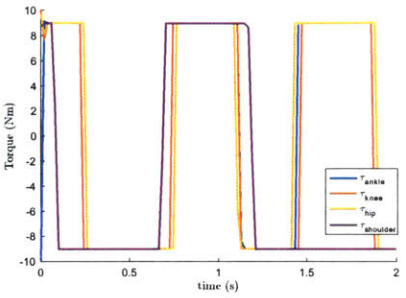

(c) Optimized torque output.

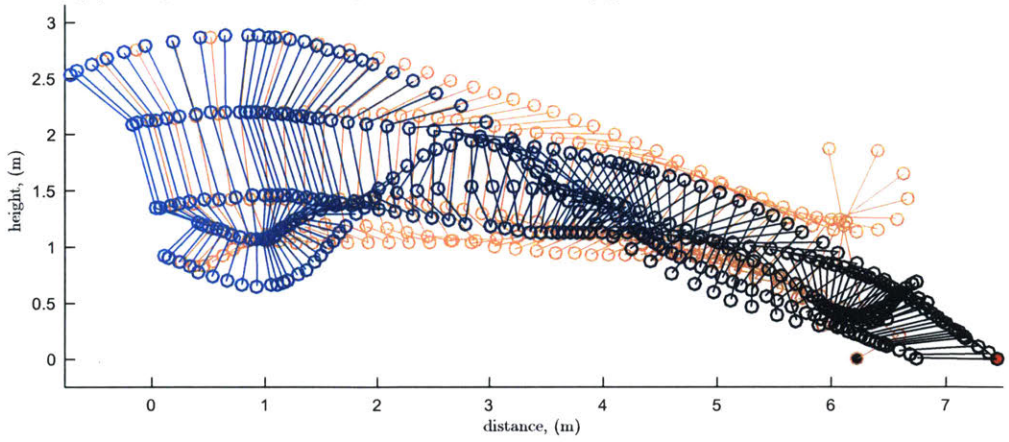

(d) Optimized trajectory.

Figure 4-1: **Physically feasible result of an optimized hitchkick jump.** An optimized jump, landing on the foot, of a hitchkick-seeded jump with a distance of 7.13m given torque limits of [-10, 10]Nm and an angle penalty multiplier of 1. The orange time-lapse represents the initial seed trajectory, blue represents the optimized time-lapse; the black dot is the initial landing point, and the red dot is the optimized one. (a) Original trajectory taken from averaging four data sets. Black represents the centers of mass. (b) Angle fits of the four joints, over 4 data sets. (c) Torque output of optimized trajectory. Torques max out at 10Nm, since the limits were set as such. (d) Optimized trajectory, one of the smoothest and most feasible results.

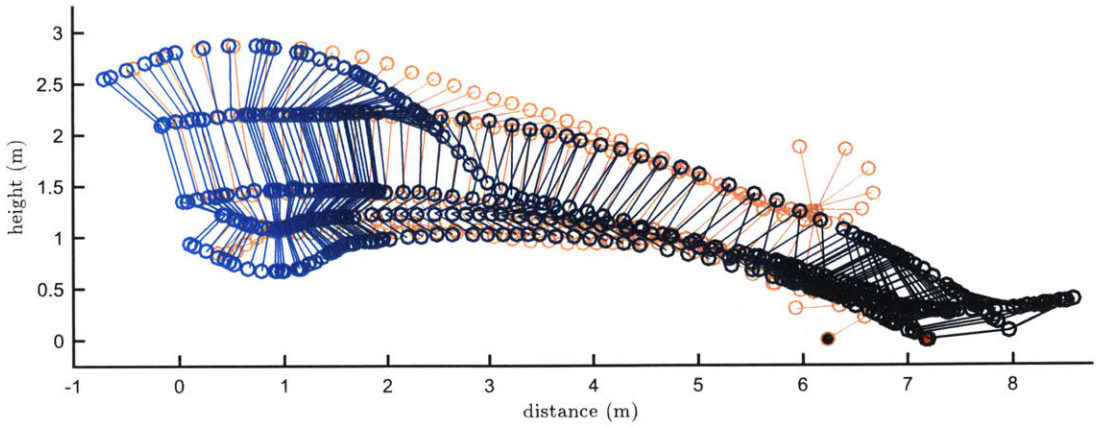

(a) Hitchkick optimization.

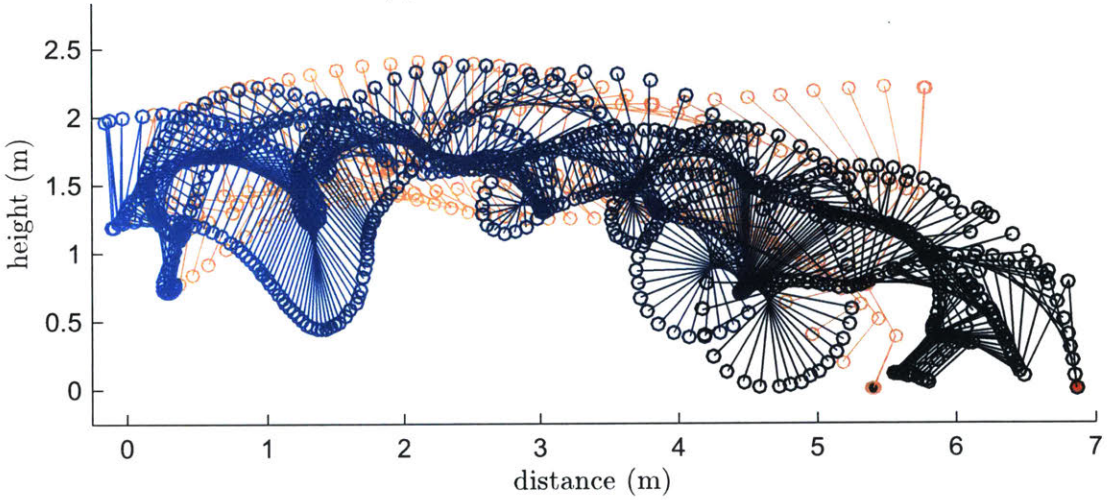

(b) Hang optimization

Figure 4-2: **Hitchkick optimization compared to hang optimization.** Both trajectories had torque limits of [-10, 10]Nm and angle penalties of 1E4. Orange timelapse represents the initial seed trajectory, blue represents the optimized timelapse; the black dot is the initial landing point, and the red dot is the optimized one. The hitchkick model and optimizer worked much better across most of the penalties and limits set, with an average of 7.7% increase, whereas the hang technique averaged a 15.89% *decrease* over the same range of limitations. Clearly, the hang technique optimizer creates physically impossible plots.

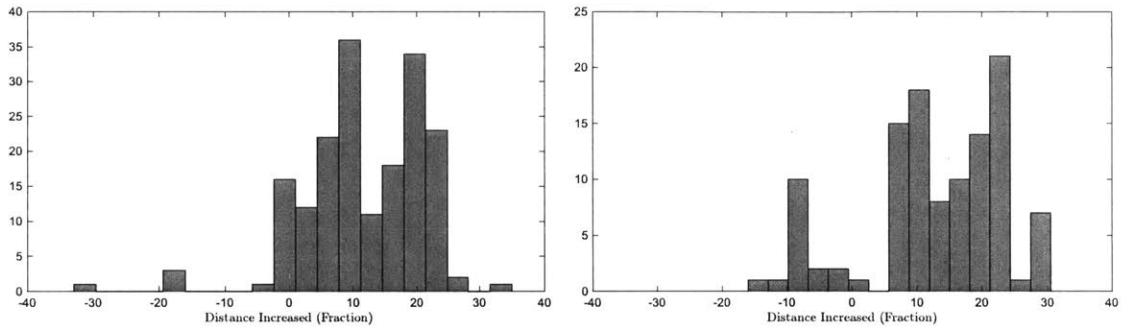

(a) Hitchkick Histogram.

(b) Hang Histogram

Figure 4-3: **Histogram of hitchkick and hang results.** Results of the simulations run based on torque limits ranging from [-5, 5] to [-2000, 2000] and angle multipliers ranging from 1E-6 to 1E8. For the hitchkick seed, n=181, and for the hang, n=111. Despite having a larger range, the hitchkick optimizer performed better overall compared to the hang optimizer, averaging a 7.7% increase compared to a 15.89% decrease.

Chapter 5

Conclusions and Future Work

Although the hang technique is simpler and theoretically easier to simulate, its simplicity may have caused the resulting trajectories to contort to an extreme extent. On the other hand, the hitchkick technique was capable of optimizing to smooth trajectories given tight torque limits, and consistently improved distances by over 20%.

Optimization clearly proved to be tricky, given the non-linear nature of the dynamics. This was evident in the initial spread of the testing parameters, where there was no clear minimum and likely many local minima in the cost function. In addition to reconsidering and optimizing the parameters themselves, further work could be done in categorizing the best parameters for different techniques, and not just for an individual.

One major flaw in the model is that it calculates the distance travelled based on the first point of contact with the ground. This disregards the rest of the body, and in the case of nearly-horizontal landing, another part of the body will likely touch the ground closer to the board, shortening the distance measured. Future simulations could consider the entire landing by adding a reaction force once the body breaks the ground plane, forcing the body to slide horizontally. Additionally, the distance measured could be that of the last body segment to pass through the ground plane. This would assume a lack of friction in the horizontal direction when the jumper lands in the sand, which may be a non-negligible factor in the methods used today.

Given some of these humanly impossible trajectories, a robot could be designed to meet that criteria and execute the optimized jumps without a problem. By eliminating the limitations of the human body, this model could be applied to machines to enhance performance. Although bipedal robots are hardly past the stage of simple locomotion, enabling such machines to do as much and more than a human opens the door to a more functional machine that may actually make an impact on society.

Appendix A

Anthropomorphic Data for the Human Body

To find the center of mass, the mass was multiplied by the COM fraction from Table A.1. For the center of mass of an entire system of n links,

$$x = \frac{1}{M} \sum_{i=1}^{n} m_i x_{ci}$$

with M being the total mass, m the mass of the specific link, and x_c the COM distance for that link.

Moment of inertia was also calculated:

$$I = \sum_{i=1}^{n} m_i x_{ri}^2$$

with x_r representing the radius of gyration of the link. [12]

Segment	Segment Weight/ Total Body Weight	COM/Segment Length (Proximal)	Radius of Gyration (Proximal)
Head & Neck	0.081	1.000	0.116
Upper Arm	0.028	0.436	0.542
Forearm & Hand	0.022	0.682	0.827
Trunk	0.497	0.500	-
Thigh	0.100	0.433	0.540
Foot & Leg	0.061	0.606	0.735
Total Arm	0.500	0.530	0.645
Trunk, Head, & Neck	0.578	0.660	0.830

Table A.1: Anthropomorphic Data.

Appendix B

Dynamics of a four-link unconstrained uystem

The flight phase dynamics, taken from Hyon, et al, were derived for a four-linked robot [7]. Assuming the kinetic energy of the four-linked system is $K = \frac{1}{2}\dot{q}^{\,T} J(q)\dot{q}$, this can be converted to q_g as follows:

$$K = \frac{1}{2}\dot{q}^T J q \dot{q} = \frac{1}{2}\dot{q_g} R(\theta)\dot{q} = \frac{1}{2}\dot{q_g} J_g(\theta)\dot{q_g} \tag{B.1}$$

Converting the center of mass position to the ankle position can be done by multiplying $[x_0, y_0]$ by the rotation matrix:

$$\begin{bmatrix} x_g \\ y_g \end{bmatrix} = \begin{bmatrix} x_0 \\ y_0 \end{bmatrix} - \frac{1}{M} \begin{bmatrix} b_1 c_1 + b_2 c_{12} + b_3 c_{123} + b_4 c_{1234} \\ b_1 s_1 + b_2 s_{12} + b_3 s_{123} + b_4 s_{1234} \end{bmatrix}$$

$$M = m_1 + m_2 + m_3 + m_4$$

$$b_1 = -m_1 l_{c1} - (m_2 + m_3 + m_4) l_1$$

$$b_2 = -m_2 l_{c2} - (m_3 + m_4) l_2$$

$$b_3 = -m_3 l_{c3} - m_4 l_3$$

$$b_4 = -m_4 l_{c4}$$

$$s_{12\cdots} = sin\,(\theta_1 + \theta_2 + \cdots)$$

$$c_{12\cdots} = cos\,(\theta_1 + \theta_2 + \cdots)$$

The inertial matrix, J_g, is as follows:

$$J_g(\theta) = \begin{bmatrix} M & 0 & 0 & 0 & 0 & 0 \\ 0 & M & 0 & 0 & 0 & 0 \\ 0 & 0 & J_{g33} & J_{g34} & J_{g35} & J_{g36} \\ 0 & 0 & J_{g34} & J_{g44} & J_{g45} & J_{g46} \\ 0 & 0 & J_{g35} & J_{g45} & J_{g55} & J_{g56} \\ 0 & 0 & J_{g36} & J_{g46} & J_{g56} & J_{g66} \end{bmatrix}$$

$J_{g33} = 2(k_5 c_2 + k_6 c_3 + k_7 c_4 + k_8 c_2 3 + k_9 c_3 4 + k_{10} c_2 34 + k_{11} s_2 + k_{12} s_{23} + k_{13} s_{234}) + k_1 + k_2 + k_3 + k_4,$

$J_{g34} = k_5 c_2 + 2k_6 c_3 + 2k_7 c_4 + k_8 c_{23} + 2k_9 c_{34} + k_{10} c_{234} + k_{11} s_2 + k_{12} s_{23} + k_{13} s_{234} + k_4 + k_2 + k_3,$

$J_{g35} = k_6 c_3 + 2k_7 c_4 + k_8 c_{23} + k_9 c_{34} + k_{10} c_{234} + k_1 2 s_{23} + k_1 3 s_{234} + k_4 + k_3,$

$J_{g36} = k_7 c_4 + k_9 c_{34} + k_{10} c_{234} + k_{13} s_{234} + k_4,$

$J_{g44} = 2k_6 c_3 + 2k_7 c_4 + 2k_9 c_{34} + k_2 + k_3 + k_4,$

$J_{g45} = k_6 c_3 + 2k_7 c_4 + k_9 c_{34} + k_3 + k_4,$

$J_{g46} = k_7 c_4 + k_9 c_{34} + k_4,$

$J_{g55} = 2k_7 c_4 + k_3 + k_4,$

$J_{g56} = k_7 c_4 + k_4,$

$J_{g66} = k_4,$

with

$$k_1 = (Ma_{11}b_1^2)/M,$$

$$k_2 = (Ma_{22}b_2^2)/M,$$

$$k_3 = (Ma_{33}b_3^2)/M,$$

$$k_4 = (Ma_{44}b_4^2)/M,$$

$$k_5 = (b_5b_2)/M,$$

$$k_6 = (Ma_{14}b_2b_3)/M,$$

$$k_7 = (Ma_{23}b_4b_3)/M,$$

$$k_8 = (b_5b_3)/M,$$

$$k_9 = (Ma_{45}b_2b_4)/M,$$

$$k_{10} = (b_5b_4)/M,$$

$$k_{11} = (Ma_{25} + b_1b_2)/M,$$

$$k_{12} = (Ma_{34} + b_1b_3)/M,$$

$$k_{13} = (Ma_{35} + b_1b_4)/M,$$

$$a_{14} = (m_3l_{c3} + m_4l_3)l_2,$$

$$a_{23} = m_4l_{c4}l_3,$$

$$a_{25} = (m_2l_{c2} + m_3l_2 + m_4l_2)\,l_1,$$

$$a_{34} = (m_3l_{c3} + m_4l_3)\,l_1,$$

$$a_{35} = m_4l_{c4}l_1,$$

$$a_{11} = I_1 + m_1l_{c1}^2 + (m_2 + m_3 + m_4)\,l_1^2,$$

$$a_{22} = I_2 + m_2l_{c2}^2 + (m_3 + m_4)\,l_2^2,$$

$$a_{33} = I_3 + m_3l_{c3}^2 + m_4l_3^2,$$

$$a_{44} = I_4 + m_4l_{c4}^2,$$

$$a_{45} = m_4l_{c4}l_2.$$

Lengths l and l_c represent length of respective link and distance from rotation to the center of mass for each link, respectively, which can be found in Table 3.1.

Using Lagrange's equations of motion, where the only source of potential energy is from gravity,

$$\frac{d}{dt}\left(\frac{\partial K}{\partial \dot{q}_g}\right) - \frac{\partial K}{\partial q_g} + G_g = u \tag{B.2}$$

where G_g is the gravitational vector,

$$G_g(q_g) = \begin{bmatrix} 0 \\ Mg \\ 0 \\ 0 \\ 0 \\ 0 \end{bmatrix}$$

with

$$\frac{d}{dt}\left(\frac{\partial K}{\partial \dot{q}_g}\right) = J_g(q_g)\ddot{q}_g + \frac{d}{dt}J_g(q_g)\dot{q}_g \tag{B.3}$$

and

$$H_g(q_g, \dot{q}_g) = \frac{d}{dt}J_g(q_g)\dot{q}_g - \frac{\partial K}{\partial q_g} \tag{B.4}$$

resulting in:

$$J_g(q_g)\ddot{q}_g + H_g(q_g, \dot{q}_g) + G_g(q_g) = u \tag{B.5}$$

Bibliography

[1] K. Arikawa and T. Mita. Design of multi-DOF jumping robot. volume 4, pages 3992–3997. IEEE, 2002.

[2] Blake M. Ashby and Jean H. Heegaard. Role of arm motion in the standing long jump. *Journal of biomechanics*, 35(12):1631–1637, 2002.

[3] H Hatze. A comprehensive model for human motion simulation and its application to teh take-off phase of the long jump. *Journal of Biomechanics*, 14(3):135–142, 1981.

[4] James G. Hay. Citius, altius, longius (faster, higher, longer): the biomechanics of jumping for distance. *Journal of biomechanics*, 26:7–21, 1993.

[5] James G. Hay, John A. Miller, and Ron W. Canterna. The techniques of elite male long jumpers. *Journal of biomechanics*, 19(10):855–866, 1986.

[6] H. Hemami and B. Wyman. Modeling and control of constrained dynamic systems with application to biped locomotion in the frontal plane. *IEEE Transactions on Automatic Control*, 24(4):526–535, August 1979.

[7] Sang-Ho Hyon, Naoto Yokoyama, and Takashi Emura. Back handspring of a multi-link gymnastic robot reference model approach. *Advanced Robotics*, 20(1):93–113, January 2006.

[8] T. R. Kane and M. P. Scher. A dynamical explanation of the falling cat phenomenon. *International Journal of Solids and Structures*, 5(7):663IN1667–666IN2670, 1969.

[9] Thomas R. Kane and M. P. Scher. Human self-rotation by means of limb movements. *Journal of biomechanics*, 3(1):39–49, 1970.

[10] Xiuping Mu. *Dynamics and Motion Regulation of a Five-link Biped Robot Walking in the sagittal plane.* PhD thesis, The University of Manitoba, 2004.

[11] A Seyfarth, A Friedrichs, V Wank, and R Blickhan. Dynamics of the long jump. *Journal of Biomechanics*, 32:1259–1267, 1999.

[12] David A. Winter. *Biomechanics and motor control of human movement.* Wiley, Hoboken, N.J, 4th ed edition, 2009. OCLC: ocn318408191.